A Systematically Generated, Pressure-Dependent Mechanism for High-Conversion Ethane Pyrolysis. 1. Pathways to the Minor Products

David M. Matheu*,† and Jeffrey M. Grenda‡

National Institute of Standards and Technology, Gaithersburg, Maryland 20899, and ExxonMobil Research and Engineering Company, Annandale, New Jersey 08801

Received: October 21, 2004; In Final Form: February 21, 2005

The deposition of carbon during hydrocarbon pyrolysis is part of many industrial processes. The rate and nature of deposition depend, in part, on the gas-phase chemistry of the minor pyrolysis products, which serve as deposition precursors. But the specific reaction pathways governing the formation and destruction of these minor gas-phase products are only partially known. We apply an updated version of our automated mechanism generation tool XMG-PDep to the high-conversion, pyrocarbon-depositing ethane pyrolysis system of Glasier and Pacey, to systematically uncover the likely reaction pathways governing the observed minor products acetylene, propylene, 1,3-butadiene, and benzene. Thorough examination by means of sensitivity, equilibrium, and reaction-pathway analyses reveals an extremely complex, intertwined set of reaction pathways controlling these deposition precursors, some of which are not often considered in the wider pyrolysis literature. Large, aggregated sets of disproportionation reactions, for example, appear to play an important role in the formation of benzene. The analyses motivate a companion paper (following paper in this issue) which explores in greater depth the effects of large groups of radical disproportionation reactions, omitted reaction families, and the possibility that pressure changes in the reactor could alter the distribution of the deposition precursors.

1. Introduction

Manufacturers turn to hydrocarbon pyrolysis to form orderly deposits of carbon material, called pyrocarbon, for use in a variety of applications from aircraft disk brakes to nuclear fuel pellet coatings. In these pyrolysis systems, the detailed gas-phase chemistry has important effects on the quality of the carbon deposited and the rate of deposition.[1] Pyrolytic carbon deposition also remains a key challenge for the industrial cracking of light alkanes, and the minor gas-phase products of the alkane pyrolysis can be important intermediates on the path to deposited material (see, e.g., refs 2 and 3). But under many pyrolysis conditions, the gas-phase chemistry which controls the minor products, or deposition precursors, is not well-described at a mechanistic level.

In a recent attempt to learn more about the influence of major and minor pyrolysis products on pyrocarbon deposition rates, Glasier and Pacey studied neat ethane pyrolysis at very high conversion (900−1200 K, 0.4 bar, conversion >98%) in a specially equipped flow reactor.[4] Unlike conventional ethane pyrolysis, in which ethane conversion may reach 70%, the Glasier and Pacey high-conversion experiments involve an extremely large number of products, intermediates, and pathways. The large number of participating species and reactions makes developing an appropriate detailed chemical kinetic model extremely difficult; to our knowledge, no published model exists which is suited to the conditions of the experiments. The pressure dependence of many reactions in the Glasier and Pacey system also thwarts model development, in particular frustrating numerical algorithms that might otherwise be used to build a pyrolysis mechanism automatically.

* To whom correspondence should be addressed. Present address: Cabot Corp., Billerica, MA 01821. E-mail: dmatheu@cabot-corp.com.
† National Institute of Standards and Technology.
‡ ExxonMobil Research and Engineering Co.

That is unfortunate, since detailed knowledge of how the minor products of high-conversion ethane pyrolysis form and decompose could contribute to our ultimate understanding of how the larger aromatic species are produced in this and similar pyrolysis systems—an area of continuing research. Furthermore, if the minor gas-phase product concentrations eventually affect the rate and character of the deposited pyrocarbons, then knowledge of how they form is required for the predictive and transferable modeling of the deposition process as a whole.

To address this problem, we modify and apply the automated mechanism generation tool XMG-PDep,[5,6] to systematically build a gas-phase mechanism for the challenging conditions of the Glasier and Pacey experiments. The resultant kinetic model is strictly elementary-step-based and includes a general treatment of reaction pressure dependence, including multichannel pressure-dependent reactions. Using this model, we identify key pathways governing the formation and destruction of the observed minor products acetylene, propylene, 1,3-butadiene, and benzene, by combining detailed equilibrium, sensitivity, and reaction pathway analyses.

Many of the reaction routes we identify in this way are already well-known in the pyrolysis and combustion literature, but others are not often discussed, and their pressure-dependent character is rarely addressed. Moreover, the comprehensive picture revealed here is one of great complexity in the gas-phase chemistry, involving whole collections of parallel, intertwined pathways to all of the minor products.

2. Computational Method: XMG-PDep

2.1. Automated Mechanism Generation with Pressure Dependence. XMG-PDep is a software tool for building complex chemical kinetic models using mathematical matrix methods. It is based on XMG,[7,8] which in turn was developed

10.1021/jp0451804 CCC: $30.25
Published on Web 05/26/2005

from NetGen.[9−12] A complete description of the algorithm, and the details of its application, are presented in ref 5; this section provides a brief review. The next section describes the changes to XMG-PDep required for accurate treatment of the Glasier and Pacey experiments.

XMG-PDep uses a set of "reaction families" to generate all the possible reactions of a given chemical species by itself and with other species in the mechanism. Each reaction family represents a particular type of elementary-step chemical reaction, such as bond-breaking or radical addition to a double bond. Application of the families to a particular species produces new reactions. It also produces new species, which become candidates for further generation of reactions. The new reactions are added to the continuously developing chemical kinetic model, which is complete when certain reaction-flux-based criteria are established.

Pressure-dependent reactions are constructed using partial pressure-dependent networks.[13,14] Each partial network contains a small, screened version of the full pressure-dependent network that would be produced if all possible isomerizations and decompositions of the species in the network were allowed. The partial network includes enough detail to allow reasonable predictions of $k(T,P)$ for each reaction in it.[13] A "leakage flux" is also evaluated, which describes the total chemical flux to all portions of the partial network not yet included in the model.

XMG-PDep grows the chemical mechanism iteratively, one species or pressure-dependent network at a time. At each iteration, the generation algorithm decides what to explore next by constructing from the current mechanism the set of ordinary differential equations (ODEs) representing the evolution of the chemical system in time, at a single temperature and pressure, specified by the user. It solves these ODEs and examines all the fluxes to those species not yet included in the mechanism, and to the nonincluded portion of each pressure-dependent network. It chooses that species or pressure-dependent network with the largest flux, using the reaction families, and explores its reactions. It then adds the appropriate species and/or reactions to the kinetic model. The process is complete when XMG-PDep can solve the ODEs to a user-specified conversion, with all fluxes to nonincluded parts of the mechanism less than the scaled flux criterion R_{min}, over the entire integration time t. The flux criterion R_{min} is given by

$$R_{min}(t) = f_{min} R_{char}(t) \tag{1}$$

$R_{char}(t)$ is the characteristic rate for the whole mechanism at time t, as given by Song et al.[15]

$$R_{char}(t) = [\sum_j R_{reacted(j)}{}^2(t)]^{1/2} \tag{2}$$

and f_{min} is a user-specified tolerance, typically 0.1−1%. $R_{reacted(j)}(t)$ represents the net rate of change of each species already in the mechanism.

Rate constants for each of the discovered reactions are drawn from a literature library where available, but most often come from a set of structure-based reaction rate estimation rules. These are usually modified Arrhenius forms for specified subfamilies of reactions (e.g., "1,4 internal H-abstractions from a primary to a secondary radical"). The QRRK code CHEMDIS[16] and density-of-states code THERFIT[17] provide estimates of the rate constants $k(T,P)$ for pressure-dependent reactions where values are not available from the literature, using the rate rules as inputs. Similarly, the thermochemical data needed to ensure thermodynamic consistency, and to produce a CHEMKIN-formatted[18,19] output file of the mechanism, are drawn from an electronic library if possible. When library data are not available, the mechanism generation algorithm uses GAPP[7,8] to predict thermochemical properties via group-contribution methods.

2.2. Required Additions to the XMG-PDep Algorithm. *2.2.1. Plug Flow Reactor at Constant Pressure*. To build the governing differential equations required to estimate transient species concentrations and fluxes during mechanism generation, XMG-PDep must implicitly assume a reactor model. Earlier versions assumed a simple, perfectly mixed batch reactor at constant temperature, pressure, and volume.[6] With these assumptions the gas-phase differential equation for species concentrations is

$$\frac{dC_j}{dt} = r_j \tag{3}$$

where C_j is the concentration of species j and r_j is the net rate of chemical production of species j from all reactions in the mechanism.

The above model was appropriate for well-mixed contact conditions in which changes are considered in a closed reactor volume. But the Glasier and Pacey experiments involve very high conversion in a tubular reactor, during which the specific volume roughly doubles due to the change in the number of moles of the global reaction of ethane:

$$C_2H_6 \rightarrow H_2H_4 + H_2$$

We therefore modified XMG-PDep's reactor model to allow the total volume to change, so that the concentration equation becomes, at constant temperature and pressure

$$\frac{dC_j}{dt} = r_j - C_j\left(\frac{RT}{P}\right)\sum_i r_i \tag{4}$$

where T and P are the temperature and pressure, respectively. This formulation is equivalent to that for a plug flow reactor at constant temperature and pressure.

2.2.2. Representing k(T,P) Over a Temperature Range. CHEMDIS was used in this work to fit modified Arrhenius forms to $k(T,P)$ values at constant pressure over a limited temperature range, as in Dean.[20] The fitted Arrhenius parameters for $k(T,P)$ have no physical meaning and are particular to a specific pressure, but as a fitting form they allow accurate reproduction of calculated $k(T,P)$ values (within 20% of the actual CHEMDIS evaluations at specific T and P). This representation provides a simple way for XMG-PDep to build a CHEMKIN-style[18] input file to represent its mechanism, using "pressure-dependent" rate constants that are valid for one pressure but span a temperature range.

2.2.3. Improvements to the Group Additivity Code GAPP. Changes to the group-contribution thermochemistry code GAPP[7,8] included the addition of updated group data for specific species, such as resonantly stabilized cyclic radicals. The known difficulties in GAPP discussed earlier[6] were also addressed. The group additivity estimates of molecular collision diameter and Lennard-Jones well depth, required for the pressure-dependent reaction rate estimation methods, were improved. Additional improvements were made in the appropriate assignment of external symmetry values, which enhanced accuracy in the estimation of entropies.

2.3. Updated Reaction Families, Rate Rules, and Thermochemical and Kinetic Data. *2.3.1. Reaction Families*. The set of reaction families for this application is identical to that

TABLE 1: High-Pressure-Limit Rate Rules Added to the Set of Table 2 in Ref 6 for Application of XMG-PDep to the High-Conversion Ethane Pyrolysis Experiments[a]

rate rule	*A*	*n*	E_a	ref
C_2H_3 radical addition				
C_2H_3 addition to any double bond	7.2E+11	0	21	25
C_2H_3 addition to any triple bond	1.5E+12	0	25	26
cyclic β-scissions				
cyclopropyl (endo) ring opening	7.1E+12	0	92	27
cyclopropyl (exo) ring opening	7.1E+12	0	30	28
cyclobutyl (endo) ring opening	6.1E+10	0.8	108	14
Cyclobutyl (exo) ring opening	4.0E+12	0	51	29

[a] The cyclic radical ring-opening rate rules are explained in detail in ref 14 but were not used in the methane pyrolysis application.[6] Units of *A* are $cm^3/(mol\ s\ K^n)$; E_a units are kJ/mol

used for methane pyrolysis, given in Table 1 of ref 6, with the exception that 1,3 and 1,4 intraradical additions, and their corresponding ring-opening β-scission reverse reactions, were included here. Certain known reaction types, proceeding through diradical intermediates or via concerted and molecular pathways, were omitted from the set of reaction families, for the same reasons as were given in our earlier work.[6]

2.3.2. Thermodynamic Data Library. Thermodynamic parameters for 39 species were adapted, in part or wholly, from the literature. Most of these parameters are those used in the methane pyrolysis application, but data for a few additional species important to the Glasier and Pacey system have been added to XMG-PDep's electronic library. These are described in the Supporting Information.

2.3.3. Rate Constant Library. XMG-PDep uses literature values for the rate constant $k(T)$ or $k(T,P)$ of a reaction, when these are supplied in its electronic library. It will similarly use literature values of the high-pressure-limit rate constant $k^\infty(T)$ as inputs to CHEMDIS $k(T,P)$ estimation, where possible. In the current work about 50 such rate constants were taken from the literature and are listed in the Supporting Information.

2.3.4. Rate Rules. For most reaction steps XMG-PDep must use rate rules to estimate the rate constants; if the reaction is pressure-dependent, the rate rule is a "high-pressure-limit" rate rule and serves as an input to a CHEMDIS calculation of $k(T,P)$. This work used the rate rules from our methane pyrolysis study,[6] but with changes and additions as given in Table 1 and described below.

The special importance of vinyl radical addition to the kinetic model for the Glasier and Pacey conditions led us to update our rate rules for these reactions. Earlier applications of XMG-PDep used a generic hydrocarbon radical addition rate rule[6,21] for all vinyl addition reactions, but literature data suggest this rule is too slow to represent high-pressure-limit vinyl radical additions. In particular the experimental results of Fahr and Stein[22] and Benson and Haugen[23] and the analysis of Tsang and Hampson[24] suggest that the rate for the pressure-dependent reaction over the temperature range of 1000−1800 K and at

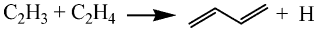

various pressures is higher than our earlier generic, high-pressure-limit rate rule by at least an order of magnitude (the high-pressure-limit rate sets an upper bound for the actual rate of any pressure-dependent reaction).

We thus added rate rules for vinyl radical addition to double bonds on the basis of the recommended rate of Tsang for vinyl addition to propene.[25] The rate rule for vinyl addition to triple bonds reflects the rate of vinyl addition to acetylene measured by Knyazev et al.[26]

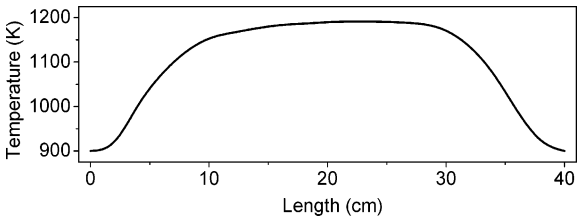

Figure 1. Temperature profile used to model the high-conversion experiments, adapted from the experimental profile of Glasier.[30] Length along the reactor is indicated on the *x*-axis.

2.4. Mechanism Generation for a Temperature Range. In the Glasier and Pacey experiments, the temperature ranges from 900 K or lower at the reactor entrance to nearly 1200 K in the middle of the reactor, with an "average" temperature of 1185 K,[4] as illustrated in Figure 1. Unfortunately, although it can *represent* reaction rate constants $k(T)$ or $k(T,P)$ over a temperature range, the XMG-PDep generation algorithm uses a single temperature and pressure when building the kinetic model. This is problematic, because an XMG-PDep-generated mechanism for the above system, using 900 K as the temperature, will be different from one generated at the average temperature of 1185 K. The set of key reactions and species changes as temperature increases, so the mechanism generator will give different "answers" for the kinetic model at different temperatures. What is desired, however, is a single kinetic mechanism which will capture all of the important chemistry from 900 to 1200 K, for use in modeling the experimental reactor.

To address this problem, we used XMG-PDep to generate ethane pyrolysis submechanisms at four different temperatures, 900, 1000, 1100, and 1185 K. We took the union of these to form a single mechanism meant to represent the pyrolysis chemistry over the whole temperature range, as described in the Appendix. We stress that this algorithmic approach to automatically generating a mechanism for a temperature range is approximate, and do not present it as a generally desirable way to model real systems. Indeed, later versions of the generation tool allow temperature and pressure to vary as specified by the user during the model construction process, eliminating the need for the ad hoc approach used here.[31]

2.4.1. Added Reaction Systems: Allene−Cyclopropene−Propyne and Propargyl + Propargyl. XMG-PDep could not construct reactions through diradical or concerted pathways; therefore, it could not discover certain important reactions on its own, such as the allene−cyclopropene−propyne isomerization system and the recombination of propargyl radicals to produce benzene or fulvene. We again used CHEMDIS to predict rate constants for the allene−cyclopropene−propyne system, on the basis of the work of Harding and Klippenstein[32] and Davis et al.,[33] this time at the experimental pressure of the Glasier and Pacey experiments and for a temperature range of 900−1200 K. The pressure-dependent isomerizations among allene, cyclopropene, and propyene, and the dissociations to propargyl radical and H-atom, were then added to the mechanism by hand.

Finally, we added a set of net pressure-dependent reactions which reflect the propargyl + propargyl network and its associated isomerizations, on the basis of the results of Miller and Klippenstein.[34] The final combined kinetic model contained approximately 5800 reactions among 126 species.

2.5. Modeling the Reactor. We used the combined kinetic model, coupled with a plug flow model[18] and an imposed temperature profile, to simulate the Glasier and Pacey experi-

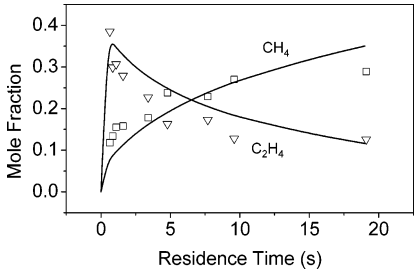

Figure 2. XMG-PDep-predicted mole fractions of methane and ethylene (lines) along with experimental data from Glasier and Pacey[4] (squares, CH_4; triangles, C_2H_4) as a function of nominal reactor residence time. Each symbol represents an experiment at a particular flow rate, expressed as a nominal residence time.

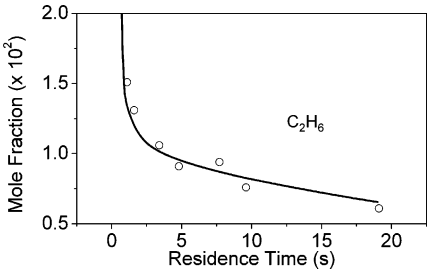

Figure 3. XMG-PDep-predicted ethane concentration (line) and experimental data (symbols) with reactor residence time.

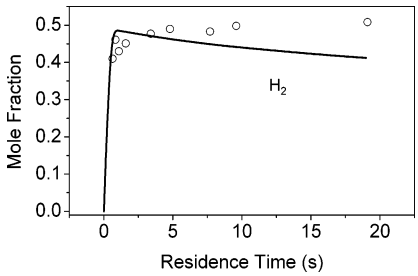

Figure 4. XMG-PDep-predicted hydrogen concentration (line) and experimental data (symbols) with reactor residence time.

ments. The reactant was neat ethane, and the reactor pressure was assumed constant at 0.4 bar. Inlet flow rates and their correspondence with nominal residence times were taken from Glasier.[30]

3. Results

Figures 2−4 compare the final mechanism's predictions of the reactant and the major product concentrations at the reactor outlet with the experimental data of Glasier and Pacey. No adjustments were made to the chemical mechanism, and no model parameters were fitted to match any of the data; the nature of the mechanism generation algorithm ensures all reactions are derived from the appropriate fundamental, elementary steps. In general, the major species predictions agree well with the experimental data, usually within 20% of the measurements, although an incorrect trend appears in the H_2 profile at longer residence times.

Figures 5−8 present predictions of the minor product concentrations. Agreement with the experimental data is acceptable—within a factor of 3—considering that no parameter adjustment is employed to fit the data, and that the absolute concentration values are small. The model captures the correct plot shape for each minor species. Even so, 1,3-butadiene concentrations are overpredicted, the peak propylene concentration is underpredicted, and the benzene concentration is

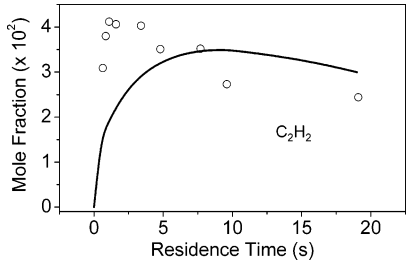

Figure 5. Predicted acetylene concentration (line) with residence time versus experimental data (symbols).

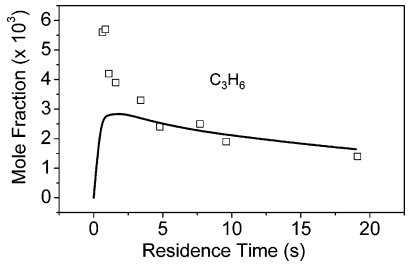

Figure 6. Predicted propylene concentration (line) with residence time versus experimental data (symbols).

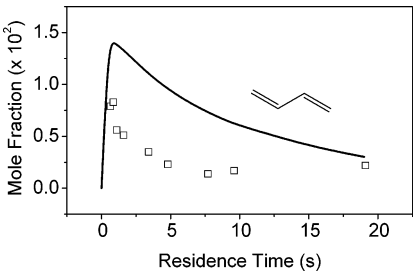

Figure 7. Predicted 1,3-butadiene concentration with residence time versus experimental data (symbols).

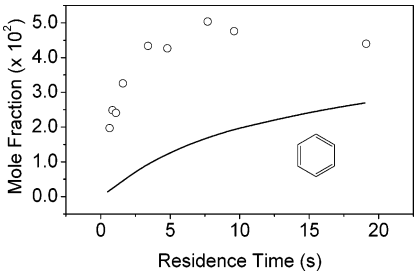

Figure 8. Predicted benzene concentration with residence time vs experimental data (symbols).

systematically underpredicted. Possible explanations for the underprediction of benzene are discussed in the companion paper of this work (following paper in this issue).

The reasonable and unfitted agreement of the generated mechanism predictions with the experimental data, found in Figures 2−8, supports the general approach of the XMG-PDep algorithm and its modifications described in this work. As in ref 6 each reaction in the combined generated mechanism is systematically based on elementary reaction steps and employs (to the best of our knowledge) reasonable, unadjusted rate rules, rate constants, and thermochemistry. The generation procedure ensures a rational search among all the possible reactions allowed by the reaction families. Figures 2−8 and the modeling approach in this work thus constitute a third pressure-dependent validation case for the continued development of the XMG-PDep algorithm and similar tools (see, e.g., ref 35).

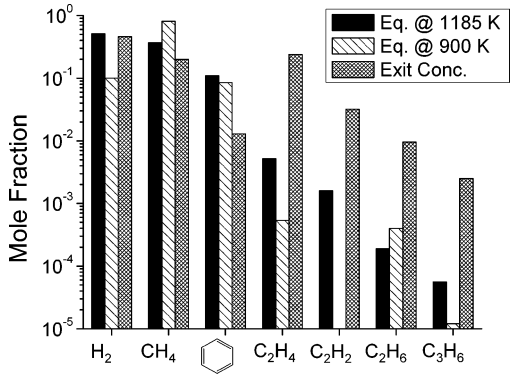

Figure 9. Predicted equilibrium mole fractions at 1185 K (reactor hot zone temperature) and 900 K (reactor exit temperature) compared to predicted mole fractions at the reactor exit for the 5 s residence time. The major products hydrogen and methane are close to their hot zone equilibrium concentrations; ethylene and the minor products are far from equilibrium.

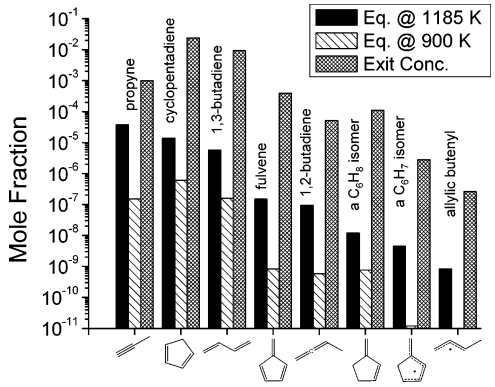

Figure 10. Continuation of Figure 9. Concentrations of these selected intermediates at the reactor outlet are much greater than the hot zone equilibrium concentrations.

4. Discussion: Pathways to the Minor Products

With over 5800 reactions, the generated mechanism is quite complex and challenging to understand or analyze. To understand the pathways governing the formation and destruction of the measured minor species acetylene, propylene, 1,3-butadiene, and benzene, we performed a reaction-pathway analysis, a calculation of equilibrium conditions, and a sensitivity analysis. As a basis we chose the model of the reactor at the 5 s nominal residence time (484 μg/s). Analytical results for this flow rate are presented below, followed by a discussion of the combined information they provide about pathways to each of the observed minor products.

4.1. Equilibrium Analysis. We used an equilibrium calculation[18] to determine how far the major and minor product concentrations might be from equilibrium at the reactor exit. Starting with neat ethane, we estimated equilibrium concentrations for all the products in the generated model, at specific temperatures and the reaction pressure (0.4 bar). Results for selected products and key intermediates are presented in Figures 9 and 10 along with the generated kinetic model predictions at the reactor exit for the 5 s nominal residence time (484 μg/s). The two temperatures represent the reactor hot zone and the reactor exit temperature.

4.2. Reaction Pathway Analysis. Figure 11 shows predicted concentrations of ethane, ethylene, and methane as a function of distance along the reactor, at the 484 μg/s flow rate. Most of the ethane is consumed by approximately 8 cm; beyond 7.5 cm the reacting system is essentially *ethylene* pyrolysis in the presence of methane and hydrogen. It is also after 7.5 cm that most of the formation and destruction of the observed minor products occurs. Few changes in any species' concentration occur beyond 30 cm due to the drop-off in temperature. We constructed a pathway analysis which focuses on this stage of the pyrolysis, from 7.5 to 30 cm, using the approach described by Racek and Burgess,[36] which we modified for this application.

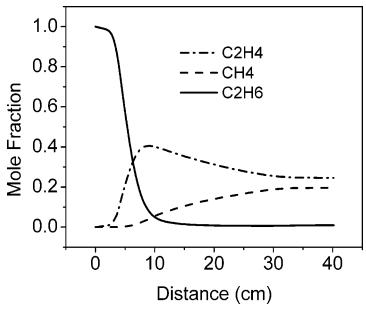

Figure 11. Predicted major species profile in the Glasier and Pacey reactor at the 5 s nominal residence time. Ethane is almost completely consumed at 7.5 cm. Beyond this point the system is effectively an ethylene pyrolysis.

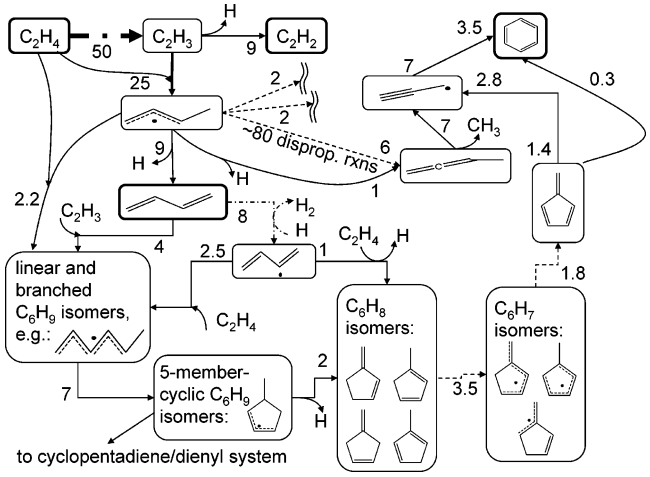

Figure 12. Partial pathway diagram for the production and consumption of minor products at the 5 s nominal residence time, within the reactor "hot zone" (from 7.5 to 30 cm). Each arrow represents either a single pathway or a collection of parallel reaction pathways of the same general type. Solid lines are net pressure-dependent pathways. Dotted lines are radical disproportionation reactions or their reverse processes. Dashed−dotted lines are radical abstraction reactions. Numbers represent integrated, net molar flux from 7.5 to 30 cm, relative to C_2H_4 consumption (=100). Arrows with two sets of numbers reflect doubling due to stoichiometric coefficients, i.e., dissociation of fulvene to two propargyl radicals. Many pathways cannot be included in this diagram; Figure 13 shows some additional pathways.

Figures 12 and 13 show the results of this pathway analysis, as integrated, *net* molar fluxes among the species from 7.5 to 30 cm at the 484 μg/s flow rate. The values in the diagrams are relative to the total consumption of ethylene (=100) over the same period. Arrows represent the direction of net flux resulting from collections of *parallel* reactions of the same type, along with their reverse reactions: e.g., disproportionation reactions and reverse disproportionations considered together.

A full diagram, considering all pathways and species separately, would be too complex to display or use; hence, some species were lumped together. These were chosen by their equivalent empirical formulas, and their apparently equivalent functions as intermediates on an eventual route to fulvene and benzene. Species within the lumped groups typically have fast reactions, or series of reactions, which connect them and cause

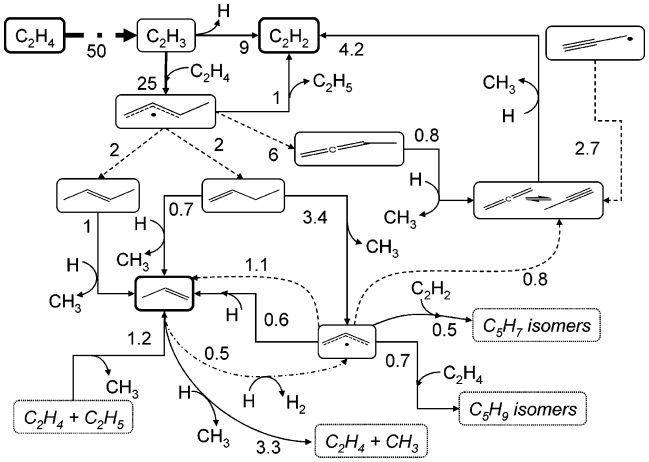

Figure 13. Continuation of Figure 12 showing additional pathways governing the fate of propylene and acetylene. The "C_5H_7 isomers" will undergo a decomposition chain similar to that of the five-membered cyclic C_6H_9 radicals in Figure 12, ending with cyclopentadiene.

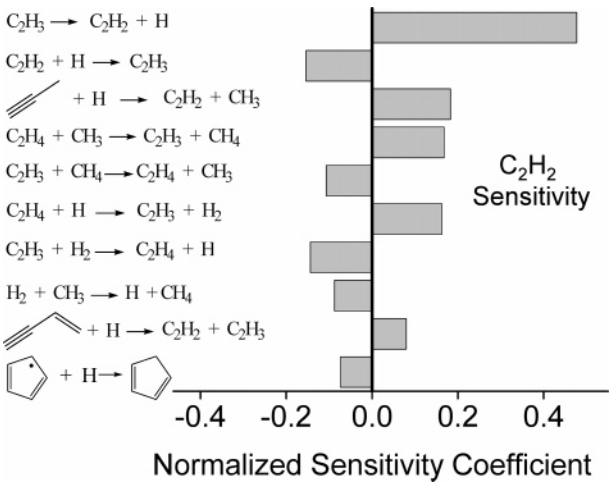

Figure 14. Normalized sensitivities for reactions contributing to acetylene at the end of the hot zone for the 484 μg/s flow rate. Except for the abstraction reactions, all of these are pressure-dependent, and some proceed through multiple isomerization steps. Reactions whose reverse instances also have high sensitivities are paired. Because the rate constants are thermodynamically consistent, forward and reverse instances of a reaction with similar absolute sensitivity coefficients indicate sensitivity to the equilibrium constant for the reaction. The primary bottleneck for acetylene formation appears to be β-scission of the vinyl radical. No single reaction appears to dominate acetylene consumption.

them to remain in relative equilibrium with each other. The lumping of species and pathways was performed *only* for aiding analysis and understanding of the reaction pathways; it was not performed for mechanism reduction (all predictions displayed in this work represent the results of the full mechanism).

4.3. Sensitivity Analysis. Neither of the previous analyses clearly identifies the rate-limiting reaction pathways for the production and consumption of the important minor products. We turned to the kinetic analysis methods of Turányi and co-workers[37] to calculate the normalized, first-order sensitivities of each reaction to each minor product. We analyzed these normalized sensitivities at the point corresponding to the end of the reactor hot zone for the 484 μg/s flow rate case (about 28 cm). Selected results are presented in Figures 14−17. Reactions are paired with their reverse instances where relevant, to show sensitivity to the equilibrium constant for the reaction.

4.4. Pathways to Measured Minor Products/Deposition Precursors. We combined the above analyses to identify

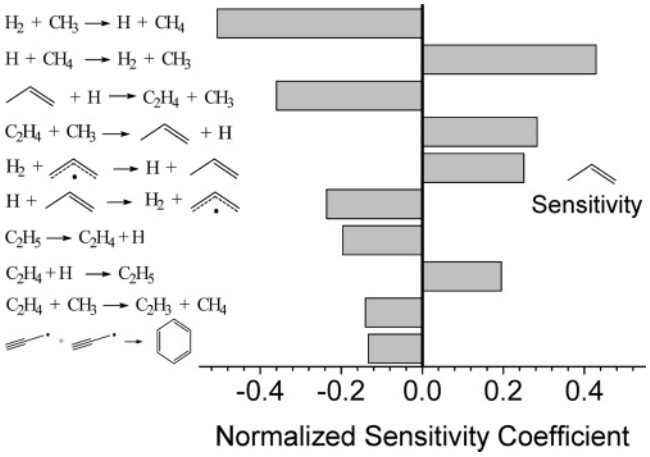

Figure 15. Normalized sensitivities for reactions contributing to propylene at the end of the hot zone for the 484 μg/s flow rate. Most of the reactions in this figure suggest that propylene concentration at the end of the hot zone is sensitive to the hydrogen atom concentration.

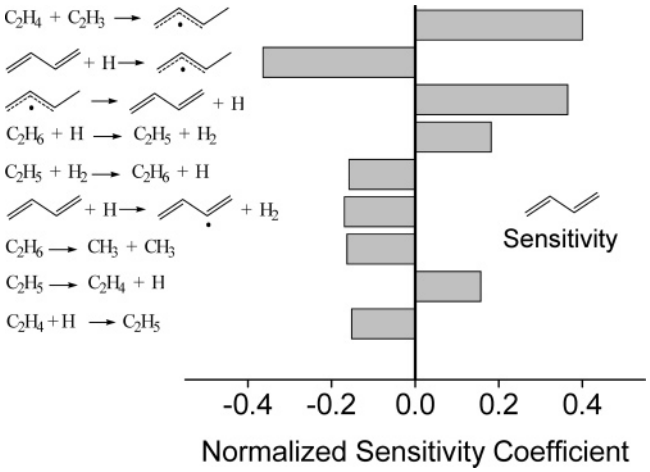

Figure 16. Normalized sensitivities for reactions contributing to 1,3-butadiene at the end of the hot zone for the 484 μg/s flow rate. Vinyl radical addition to ethylene to form the methylallyl radical appears to be a rate-limiting formation step, along with the β-scission of this radical to form 1,3-butadiene and H-atom. Note that nearly 20 reactions show significant (>0.1) sensitivity for 1,3-butadiene; only the top few reactions are shown here. The large set of disproportionation reactions which may consume methylallyl radical, as shown in Figure 12, do not appear here since no single reaction in this set has a high sensitivity by itself.

specific reactions and rate-limiting steps in our model for each of the four minor products studied (acetylene, propylene, 1,3-butadiene, and benzene). Some of these pathways are not surprising, and have been noted or alluded to in the literature for conventional ethane pyrolysis, ethylene pyrolysis, or soot and PAH formation in flames. A full comparison of our generated model to these previous studies is beyond the scope of this work, but we point out selected areas of agreement or difference with the studies of other systems. Differences do not necessarily mean disagreement; as noted by Dente and Ranzi, the relative importance of different pathways to a given minor product in pyrolysis systems can change with residence time, operating conditions, and the reacting system.[38] Many results discussed in this section are specific to the high-conversion experimental conditions of Glasier and Pacey: neat ethane pyrolyzed beyond 98% conversion at 0.4 bar and 900−1200 K.

4.4.1. Approach to Equilibrium. As is found for conventional ethane pyrolysis,[39] high-conversion ethane pyrolysis can be

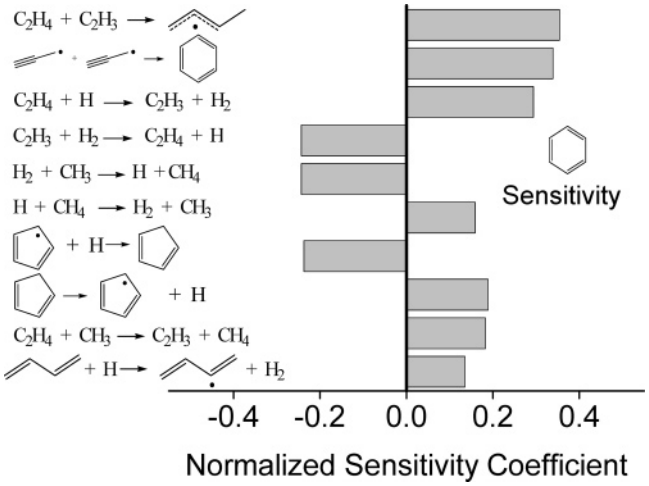

Figure 17. Normalized sensitivities for reactions contributing to benzene at the end of the hot zone for the 484 μg/s flow rate. Methylallyl formation, the recombination of propargyl radicals, and consumption of ethylene all appear to be rate-limiting.

broadly understood as a slow, kinetically controlled approach to equilibrium; in this case, however, a few species do approach equilibrium. Figures 9 and 10 immediately show that the major products hydrogen and methane are near their hot zone equilibrium concentrations. The rapid decline in temperature at the end of the reactor appears to quench the system; methane and hydrogen are "frozen" at the hot zone conditions.

None of the minor products, nor any of the intermediates that appear in the pathway diagrams of Figures 12 and 13, approach equilibrium within the hot zone (this is true even at the slowest flow rates). Benzene is the only minor product in the model whose predicted outlet concentration is significantly below its hot zone equilibrium concentration.

The overall picture provided by Figures 9, 10, 12, and 13 is therefore of ethylene product slowly converting to many minor products within the hot zone, at different rates. The minor products are themselves intermediates which do not have time to convert fully to benzene in our model. In the real system, of course, these minor products would ultimately form higher molecular weight PAHs and pyrocarbon or soot.[40]

4.4.2. Acetylene. Analysis of Figure 13 helps show how the generated model represents the formation of acetylene. In Figure 13, about half of the ethylene (C_2H_4) becomes vinyl radical (C_2H_3) through various H-abstraction reactions. Acetylene (C_2H_2) then forms by the pressure-dependent β-scission of vinyl radical. Figure 13 also reflects secondary pathways to acetylene, including multistep pressure-dependent reactions involving H addition to propyne or allene, e.g. (All multistep pressure-dependent reactions in this work are based entirely on elementary steps and take place via a partial, pressure-dependent reaction network constructed by XMG-PDep for the prediction of $k(T,P)$; see ref 14.) A third, minor pathway to acetylene involves a multistep isomerization/decomposition of the methylallyl radical.

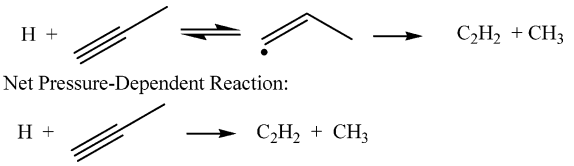

In agreement with Figure 13, the sensitivity analysis in Figure 14 suggests that pressure-dependent β-scission of the vinyl radical is the most important bottleneck to the formation of acetylene, as is found in conventional ethane pyrolysis,[39] ethylene pyrolysis,[41,42] and many small-hydrocarbon combustion systems.[43−45] The H-atom addition to propyne pathway to acetylene is also reflected in the sensitivity analysis; the third pathway of methylallyl radical decomposition is too minor to appear in Figure 14.

Finally, Figure 14 suggests acetylene concentration at the end of the hot zone is sensitive to the equilibrium

$$C_2H_4 + H \rightleftharpoons C_2H_3 + H_2$$

as well as other reactions which consume ethylene or produce vinyl radical. Since vinyl radical β-scission is the primary rate-limiting step to form acetylene, sensitivity to equilibria which strongly affect vinyl radical concentration is expected.

4.4.3. Propylene. Propylene forms by at least four important pathways, as illustrated in Figure 13. Methylallyl radical formed by the addition of vinyl to ethylene can disproportionate with other radicals to form 1-butene or 2-butene. H-atom addition to these olefins yields β-scissions to form propylene directly. Propylene also forms directly by the pressure-dependent addition of ethyl radical to ethylene, followed by β-scission, and by pathways through the allyl radical. Some of these formation pathways appear in the literature models for ethylene or conventional ethane pyrolysis (see, e.g., ref 38 or 42), but they are rarely discussed in detail, and their pressure dependence is usually ignored.

Figure 15 points to the rate-limiting step for propylene consumption: This harmonizes with Figure 13, which shows

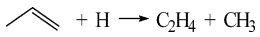

this reaction as the main consuming pathway for propylene. Figure 15 also suggests that propylene concentration is most sensitive to the equilibrium constant for the reaction

$$H + CH_4 \rightleftharpoons H_2 + CH_3$$

Given the high concentration of methane and hydrogen in the hot zone of the reactor, the above equilibrium plays a strong role in determining the ratio of H-atom to methyl radical. A shift in this equilibrium from H-atom toward methyl would simultaneously slow the rate-limiting step for propylene consumption, and promote its reverse reaction, explaining propylene's strong sensitivity to this equilibrium. Sensitivity to the equilibrated reaction

$$C_2H_5 \rightleftharpoons C_2H_4 + H$$

can be explained by the dependence of the ethyl + ethylene formation pathway in Figure 13 on ethyl radical concentration.

Propylene and the allyl radical are strongly linked by a number of pathways in Figure 13. Figure 15 points out the strongest connection, the nearly equilibrated reaction In addition

the allyl radical may go on to form C_5H_9 or C_5H_7 radicals by addition to acetylene or ethylene. These, in turn, provide secondary pathways to resonantly stabilized cyclopentadienyl radical and 1,3-cyclopentadiene (not shown).

4.4.4. 1,3-Butadiene. Much of the vinyl radical adds to ethylene to form the important methylallyl radical, as shown in Figure 12. This occurs through a multistep pressure-dependent reaction network in which the chemically activated 3-buten-1-

yl radical isomerizes to an allylic form: The subsequent

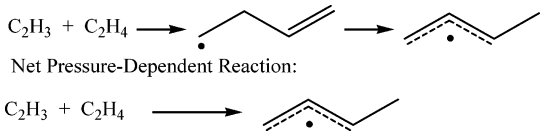

β-scission of the methylallyl radical completes the primary 1,3-butadiene formation route in our model. Figure 16 identifies this vinyl addition to ethylene to form the methylallyl radical as rate-limiting.

Many other researchers have previously identified vinyl addition to ethylene as a key step for 1,3-butadiene formation in hydrocarbon pyrolysis (for example, Weissman and Benson,[46] Roscoe et al.,[42] and Sundaram and Froment[47]), but they have only considered the 3-buten-1-yl adduct, not the allylicbutenyl radical. In their models it is the 3-buten-1-yl adduct which undergoes β-scission to form 1,3-butadiene. Additionally, the pressure dependencies of both 3-buten-1yl formation and the subsequent β-scission are usually ignored.

In fact, the vinyl radical addition to ethylene initiates a pressure-dependent network, with changing behavior at different pressures and temperatures.[14] For a given pressure, ref 14 suggests the reaction will proceed directly to 1,3-butadiene + H-atom at high temperatures. As temperature decreases, the methylallyl, and then the 3-buten-1-yl radical, dominates as the primary product of the addition.

We note, however, that which product dominates the vinyl + ethylene addition is extremely sensitive to the thermochemistry data used for the methylallyl radical. In this work we have adopted the value of Burcat[48] for this radical (ΔH_f(298 K) = 126 kJ/mol) as an improvement over our group-contribution estimate (ΔH_f(298 K) = 138 kJ/mol).[14] Figure 16 reflects this dependency on thermochemistry in the sensitivity shown toward the equilibrium

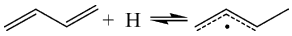

As shown in Figure 12, the 1,3-butadiene in our model is attacked mostly by H-atom abstraction, or by vinyl radical addition to form a pool of linear and branched C_6H_9 radicals (many of which are resonantly stabilized). Figure 16 reflects the 1,3-butadiene concentration's sensitivity to H-atom abstraction at the 2-position, and suggests this is the rate-limiting consumption step.

It is not clear why 1,3-butadiene is sensitive to the equilibria

$$C_2H_6 + H \rightleftharpoons C_2H_5 + H_2$$

$$C_2H_6 \rightleftharpoons CH_3 + CH_3$$

with positive sensitivity toward the $C_2H_5 + H_2$ products in the first reaction. One possibility is that since the ethyl radical undergoes β-scission to form ethylene and H-atom, it is important in providing ethylene, which is both the primary source of vinyl radical and the partner for the vinyl addition step. In addition to those steps already mentioned, at least 10 other reactions show normalized sensitivity coefficients for butadiene greater than 0.1 at these conditions. Among the reactions not shown, those which consume vinyl radical show negative sensitivity for the 1,3-butadiene concentration.

4.4.5. Benzene. The dominant pathway to benzene in the generated model begins, as it does for butadiene, with vinyl addition to ethylene (Figure 12). The resultant methylallyl radical reacts by a set of over 80 radical disproportionation pathways to form 1,2-butadiene. This species dissociates to form methyl radical and propargyl radical; the propargyl radicals finally form benzene by recombination.

An alternate, less dominant route to benzene begins with 1,3-butadiene in Figure 12. Vinyl radicals may add to the butadiene to form resonantly stabilized, branched or linear C_6H_9 isomers by a variety of pressure-dependent reaction pathways. Alternately, the 1,3-butadiene may undergo H-abstraction, with the resultant radical adding to ethylene, to form the C_6H_9 isomers. Most of these isomers will undergo intraradical addition reactions to form isomers with five-membered rings, also resonantly stabilized. These radicals, in turn, undergo β-scission or radical disproportionation to form C_6H_8 isomers such as 3-methylenecyclopentene.

These C_6H_8 isomers reverse disproportionate with each other, and with other unsaturated compounds, to form C_6H_7 radicals as shown in Figure 12. The resonantly stabilized C_6H_7 radicals (all with five-membered rings) find their way to fulvene primarily by disproportionation. Fulvene may isomerize directly to benzene, but more commonly will dissociate to propargyl radicals, which go on to form benzene.

All significant pathways to benzene in the generated model begin with vinyl addition to ethylene, and pass through propargyl recombination, as reflected in the pathway diagram (Figure 12) and sensitivity analysis (Figure 17). These are the model's primary rate-limiting steps to benzene formation, with many, intertwined pathways between. Other reactions in the sensitivity analysis imply benzene concentration depends in part on equilibria which help set the concentration of hydrogen gas:

$$C_2H_4 + H \rightleftharpoons C_2H_3 + H_2$$

$$H + CH_4 \rightleftharpoons H_2 + CH_3$$

The link to hydrogen gas concentration probably reflects the stoichiometric connection between benzene formation (or that of any hydrocarbon with a low H-to-C ratio) and hydrogen production.

Negative sensitivity to the equilibrium of may be explained

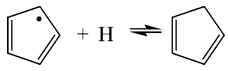

by pathways implicit in Figure 12 which draw off cyclic C_6H_9 species to form cyclopentadienyl radical. The ultimate formation of cyclopentadiene pulls molar flux along this pathway. Finally, positive sensitivity for the reaction is not surprising given Figure

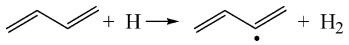

12, which shows this route as an entrant to the secondary benzene formation pathway in the model.

The importance of the vinyl + ethylene step for benzene fits numerous earlier suggestions that vinyl addition to ethylene is a bottleneck for the formation of many subsequent products in ethylene pyrolysis (see, e.g., ref 42). But the question of which reaction pathways lead to the first aromatic species under varying combustion or pyrolysis conditions is still a matter of active research. Only the so-called odd-carbon-atom pathway—propargyl radical recombination to form benzene—appears here, but XMG-PDep did test and partially explore many of the even-atom pathways discussed or reviewed by Richter and Howard,[44,49] Appel, Bockhorn, and Frenklach,[43] and Frenklach,[50] and in works referenced therein. None of the pressure-dependent networks resulting from even-atom pathways had fluxes fast

enough to be included in the model. The mechanism generation algorithm found these pathways were too slow to be explored further. The dominance of the propargyl recombination pathway in this work is specific to the experimental conditions, but it happens to match the findings of Richter and Howard for acetylene and ethylene flames,[44] and Pope and Miller for acetylene, ethylene, and propylene flames.[51]

The dominant route to propargyl radical proposed in Figure 12 is unusual, because of the collective effect of approximately 80 radical disproportionation reactions connecting methylallyl radical and 1,2-butadiene. As expected, no single disproportionation reaction from this set is important enough, by itself, to appear in a normal sensitivity analysis for benzene (Figure 17). But as a group they serve to convert products of vinyl radical addition to ethylene into propargyl radical in the model. Benzene sensitivity to these pathways considered as a group is explored in the companion paper of this work (following paper in this issue).

Finally, we note that the systematic underprediction of the benzene concentration in Figure 8 suggests that the generated model can only explain half of the experimentally observed benzene production. We speculate that this is due in part to the mechanism generator's inability to discover certain reaction types, and discuss this in the following paper in this issue. It is important to note that the systematic and meticulous method suggests that the primary and secondary pathways it *did* find, specifically those to propargyl and ultimately to benzene, are both important and reasonable for the Glasier and Pacey conditions.

5. Conclusions

We used the automated mechanism generation tool XMG-PDep to construct a chemical kinetic model "from scratch" for the complex high-conversion ethane pyrolysis system of Glasier and Pacey. It includes systematic treatment of the pressure dependence and a rational algorithm for model growth and termination. The model makes reasonable predictions for all the observed major and minor products, without adjustment or fitting of any model parameters to the experimental data.

Pathway diagrams reveal a set of complex, intertwined, parallel pathways that control the formation and destruction of each of the four observed minor products, which are all suspected as direct or indirect pyrocarbon deposition precursors. Because of the systematic and exhaustive approach to model-building, it is likely that this complexity reflects that in the natural gas-phase system.

Our model shows acetylene formation governed, unsurprisingly, by pressure-dependent vinyl radical β-scission, but identifies important secondary routes to acetylene as well. Propylene in our model is formed by at least four separate routes of roughly equal importance, with its destruction rate-limited by the pressure-dependent addition of H-atom. The H-atom/methyl radical ratio appears to control the consumption rate of propylene by this rate-limiting step.

The addition of vinyl radical to ethylene limits 1,3-butadiene formation in our model, which agrees with much prior work, but in our case the formation of methylallyl radical is dominant. Many earlier pyrolysis modeling studies have ignored this species and the general pressure dependence of the vinyl + ethylene system, which is also sensitive to the thermochemistry used to represent the methylallyl radical. Additionally, a set of about 10 reactions all show significant sensitivity for 1,3-butadiene concentration, through their effects on the vinyl radical concentration.

Benzene formation in the generated model is rate-limited by propargyl radical recombination and by vinyl addition to acetylene, with many complex, interconnected pathways connecting these initial and final steps. A set of approximately 80 radical disproportionation reactions appear to play an important role in the primary route to the propargyl radical. No single reaction in the set will appear in a sensitivity analysis; their effect is in the aggregate, and we point out that such aggregate effects in general are rarely considered seriously in model development.

The formation of resonantly stabilized, five-membered-ring C_6H_9 and C_6H_7 radicals that lead, through fulvene, to propargyl radicals represents the most important possible "alternate route" to benzene in the generated model. Although XMG-PDep can discover even-carbon-atom as well as odd-carbon-atom pathways ($C_3H_3 + C_3H_3$) to benzene, the even-carbon-atom pathways are too slow to be included by the generation algorithm.

Acknowledgment. We thank Prof. William H. Green, Jr. of the Massachusetts Institute of Technology for the use of computing facilities, as well as providing thoughtful discussion and advice. Prof. Philip D. Pacey of Dalhousie University and Dr. Greg Glasier of Wyeth Research supplied technical commentary and detailed information on their experiments. The advice and recommendations of Prof. Anthony M. Dean (Colorado School of Mines) and Dr. Wing Tsang (National Institute of Standards and Technology) are gratefully acknowledged. D.M.M. expresses gratitude to the National Research Council for funding.

Appendix: Generation of the Combined Mechanism for a Temperature Range

Mechanism generation started with the generation of four initial submechanisms, one for each temperature. Although generated at a single temperature, each of the four models had representations of its rate constants $k(T)$ and $k(T,P)$ which spanned the temperature range of 900−1200 K at a pressure of 0.4 bar. We took the union of these to create a trial mechanism for the Glasier and Pacey experiments. Next, we modeled the experimental reactor at a flow rate of 710 μg/s,[30] using the trial mechanism and the experimental temperature profile supplied by Glasier.[52] This model provided rough estimates of the concentrations of the major species (ethane, hydrogen, methane, and ethylene) at different points along the reactor.

We then repeated the four mechanism generation runs with XMG-PDep, this time using the estimated species concentrations from the trial mechanism as the initial species concentrations for generation, as listed in Table 2. At 1185 K, the extreme proliferation of species and reactions found by the generator made it impossible to proceed to the experimental ethane conversions of 99% or more, so generation at this temperature was stopped at a cumulative ethane conversion of 98.5%. We then took the union of the four mechanisms to produce a final generated mechanism for the experimental conditions, though this required a way to resolve conflicts between the submechanisms.

In each of the four submechanisms, CHEMDIS provided modified Arrhenius fits to model the behavior of $k(T,P)$ at the reaction pressure. But due to different conditions for the generation of each submechanism, the pressure-dependent networks used to predict $k(T,P)$ sometimes differed (see ref 13). For example, the mechanism generated at 900 K would produce a pressure-dependent network for vinyl addition to ethylene. The mechanism generated at 1185 K would also produce such

TABLE 2: XMG-PDep Generation Conditions for Each of the Four Submechanisms[a]

	initial concn (mole fraction)			
T (K)	C_2H_6	H_2	CH_4	C_2H_4
900	1.00	0.00	0.00	0.00
1000	0.88	0.06	0.00	0.06
1100	0.25	0.38	0.00	0.37
1185	0.02	0.43	0.12	0.39

[a] The initial concentrations for each generation step were chosen using the trial mechanism results in a plug flow reactor model of the Pacey and Glasier experiments. Total pressure was 0.4 bar, and the tolerance f_{min} was set to 0.01. Each submechanism was constructed starting from the initial concentrations out to a specific ethane conversion, which was chosen to bring the major species concentrations approximately up to those at the next temperature point. Compare with input conditions given in ref 6 for the methane pyrolysis application.

a network, but its structure, and hence the estimates of $k(T,P)$ derived from it, would differ from that at 900 K. To resolve these conflicts, we assumed a hierarchy: in cases where there were differing estimates of $k(T,P)$ for a reaction, the version generated at the higher temperature took precedence over that generated at the lower temperature. This hierarchy biases the combined model in favor of the higher temperature chemistry, but it only affects the pressure-dependent reactions whose rate constants were generated by CHEMDIS. Moreover, most of the minor species formation (and consumption) occurs at the higher temperatures; as expected, more than 80% of the total number of reactions arise from the complex chemistry the generation tool finds at the 1185 K generation step. Thus, the assumed hierarchy is a reasonable one.

This staged mechanism generation approach is approximate, and far from rigorous or ideal. The selection of the generation temperatures, the choice of a particular experimental flow rate as a base for mechanism generation, and the hierarchy favoring pressure-dependent reactions constructed at higher temperatures are all somewhat arbitrary. But key limitations prevented XMG-PDep's adaptation to changing temperature and pressure for this experimental case. Repeated trials with different variations of the staged generation approach produced little change in the predictions of the measured species.

Supporting Information Available: Libraries of data used in automated mechanism construction, including thermochemical, rate constant, and rate rule data; collisional energy transfer parameters for pressure-dependence calculations; details of allene-propyne-cyclopropene and propargyl recombination reaction systems added by-hand to kinetic model; dimensionless parameters used in analysis of reactor; selected chemical structure diagrams for ambiguous species names. This material is available free of charge via the Internet at http://pubs.acs.org.

References and Notes

(1) Oberlin, A. *Carbon* **2002**, *40*, 7−24.

(2) Wauters, S.; Marin, G. B. *Chem. Eng. J.* **2001**, *82*, 267−279.

(3) Trimm D. L. In *Pyrolysis: Theory and Industrial Practice*; Albright, L. F., Crynes, W. L., Corcoran, W. H., Eds.; Academic Press: New York, 1983.

(4) Glasier, G. F.; Pacey, P. D. *Carbon* **2001**, *39*, 15−23.

(5) Matheu, D. M. Integrated Pressure-Dependence in Automated Mechanism Generation: A New Tool for Building Gas-Phase Kinetic Models. Ph.D. Thesis, Massachusetts Institute of Technology, Cambridge, MA, 2002.

(6) Matheu, D. M.; Dean, A. M.; Grenda, J. M.; Green, W. H. Jr. *J. Phys. Chem. A* **2003**, *107*, 8552−8565.

(7) Grenda, J. M.; Bozzelli, J. W. Automated Elementary Reaction Mechanism Generation Incorporating Thermochemistry, Fall-off, and Chemical Activation Reactions of OH with Olefins. *5th International Conference on Chemical Kinetics, Book of Abstracts*, National Institute of Standards and Technology (NIST): Gaithersburg, MD, 2001; p A6.

(8) Grenda, J. M.; Androulakis, I. P.; Dean, A. M.; Green, W. H. Jr. *Ind. Eng. Chem. Res.* **2003**, *42*, 1000−1010.

(9) Susnow, R. G.; Dean, A. M.; Green, W. H.; Peczak, P.; Broadbelt, L. J. *J. Phys. Chem. A* **1997**, *101*, 3731−40.

(10) Broadbelt, L. J.; Stark, S. M.; Klein, M. T. *Comput. Chem. Eng.* **1996**, *20*, 113−129.

(11) Broadbelt, L. J.; Stark, S. M.; Klein, M. T. *Ind. Eng. Chem. Res.* **1995**, *34*, 2566−73.

(12) Broadbelt, L. J.; Stark, S. M.; Klein, M. T. *Ind. Eng. Chem. Res.* **1994**, *33*, 790−9.

(13) Matheu, D. M.; Lada, T. A.; Green, W. H.; Grenda, J. M.; Dean, A. M. *Comput. Phys. Commun.* **2001**, *138*, 237−249.

(14) Matheu, D. M.; Green, W. H. Jr.; Grenda, J. M. *Int. J. Chem. Kinet.* **2003**, *35*, 95−119.

(15) Song, J.; Stephanopoulos, G.; Green, W. H. *Chem. Eng. Sci.* **2002**, *57*, 4475−4491.

(16) Chang, A. Y.; Bozzelli, J. W.; Dean, A. M. *Z. Phys. Chem.* **2000**, *214*, 1533−1568.

(17) Bozzelli, J. W.; Chang, A. Y.; Dean, A. M. *Int. J. Chem. Kinet.* **1997**, *29*, 161−170.

(18) CHEMKIN Collection, v.3.6: R. J. Kee, F. M. Rupley, J. A. Miller, M. E. Coltrin, J. F. Grcar, E. Meeks, H. K. Moffat, A. E. Lutz, G. Dixon-Lewis, M. D. Smooke, J. Warnatz, G. H. Evans, R. S. Larson, R. E. Mitchell, L. R. Petzold, W. C. Reynolds, M. Caracotsios, W. E. Stewart, P. Glarborg, C. Wang, and O. Adigun, Reaction Design, Inc., San Diego, CA, 2000.

(19) NIST Disclaimer: Certain commercial materials and equipment are identified in this paper to specify procedures completely. In no case does such identification imply recommendation or endorsement by the National Institute of Standards and Technology, nor does it imply that the material or equipment identified is necessarily the best available for the purpose.

(20) Dean, A. M. *J. Phys. Chem.* **1990**, *94*, 1432−1439.

(21) Curran, H. J.; Gaffuri, P.; Pitz, W. J.; Westbrook, C. K. *Combust. Flame* **1998**, *114*, 149−177.

(22) Fahr, A.; Stein, S. E. *22nd Symp. (Int.) Combust.* **1988**, *22*, 1023−1029.

(23) Benson, S. W.; Haugen, G. R. *J. Phys. Chem.* **1967**, *71*, 1735−1746.

(24) Tsang, W.; Hampson, R. F. *J. Phys. Chem. Ref. Data* **1986**, *15*, 1087−1279.

(25) Tsang, W. *J. Phys. Chem. Ref. Data* **1991**, *20*, 221−273.

(26) Knyazev, V. D.; Stoliarov, S. I.; Slagle, I. R. *26th Symp. (Int.) Combust.* **1996**, *26*, 513−519.

(27) Olivella, S.; Sole, A.; Bofill, J. M. *J. Am. Chem. Soc.* **1990**, *112*, 2, 2160−2167.

(28) Smith, D. M.; Nicolaides, A.; Golding, B. T.; Radom, L. *J. Am. Chem. Soc.* **1998**, *120*, 10223−10233.

(29) Newcomb, M. *Tetrahedron* **1993**, *49*, 1151−1176.

(30) Glasier, G. F. Molecular growth, aerosol formation and pyrolytic carbon deposition during the pyrolysis of ethane at high conversion. Ph.D. Thesis, Dalhousie University, Halifax, Nova Scotia, Canada, 2000.

(31) Matheu, D. M.; Saeys, M.; Grenda, J. M.; Green, W. H., Jr. Automated Construction of Gas-Phase Kinetic Models: New Pathways for Old Problems; *AIChE Annual Meeting*, San Francisco, CA, 2003; American Institute of Chemical Engineers: New York, 2003; p 128A.

(32) Harding, L. B.; Klippenstein, S. J. *Proc. Combust. Inst.* **2000**, *28*, 1503−1509.

(33) Davis, S. G.; Law, C. K.; Wang, H. *J. Phys. Chem. A* **1999**, *103*, 5889−5899.

(34) Miller, J. A.; Klippenstein, S. J. *J. Phys. Chem. A* **2003**, *107*, 7783−7799.

(35) Song, J., Yu, J., Matheu, D. M., and Green, W. H. Jr. Manuscript in preparation.

(36) XSENKPLOT, v.1.2: J. Racek and D. R. Burgess, National Institute of Standards and Technology, Gaithersburg, MD, 1996.

(37) KINALC, v.1.8: T. Turányi and I. G. Zsely, Eotvos University, Budapest, Hungary, 2003.

(38) Dente M. E.; Ranzi, E. M. In *Pyrolysis: Theory and Industrial Practice*; Albright, L. F., Crynes, B. L., Corcoran, W. H., Eds.; Academic Press: New York, 1983; pp 133−173.

(39) McConnell C. F.; Head, W. D. In *Pyrolysis: Theory and Industrial Practice*; Albright, L. F., Crynes, W. L., Corcoran, W. H., Eds.; Academic Press: New York, 1983; pp 25−44.

(40) Benzinger, W.; Becker, A.; Hüttinger, K. J. *Carbon* **1996**, *34*, 957−966.

(41) Westbrook, C. K.; Dryer, F. L.; Schug, K. P. *19th Symp. (Int.) Combust.* **1982**, *19*, 153−166.

(42) Roscoe, J. M.; Bossard, A. R.; Back, M. H. *Can. J. Chem.* **2000**, *78*, 16−25.

(43) Appel, J.; Bockhorn, H.; Frenklach, M. *Combust. Flame* **2000**, *121*, 122−136.
(44) Richter, H.; Howard, J. B. *Phys. Chem. Chem. Phys.* **2002**, *4*, 2038−2055.
(45) Warnatz J. In *Combustion Chemistry*; Gardiner, W. J., Jr., Ed.; Springer-Verlag: New York, 1984; pp 197−360.
(46) Weissman, M.; Benson, S. W. *Int. J. Chem. Kinet.* **1984**, *16*, 307−333.
(47) Sundaram, K. M.; Froment, G. F. *Chem. Eng. Sci.* **1977**, *32*, 601−608.
(48) Burcat, A. *Third Millenium Ideal Gas and Condensed Phase Thermochemical Database for Combustion: TAE 867*; Technion/Israel Institute of Technology: Haifa, Israel, 2001.
(49) Richter, H.; Howard, J. B. *Prog. Energy Combust. Sci.* **2000**, *26*, 565−608.
(50) Frenklach, M. *Phys. Chem. Chem. Phys.* **2002**, *4*, 2028−2037.
(51) Pope, C. J.; Miller, J. A. *Proc. Combust. Inst.* **2000**, *28*, 1519−1527.
(52) Glasier, G. F. (Research Scientist, Wyeth Research, Montreal, Canada). Personal communication, 2003.